Anisotropic Electronic Correlations in the Spin Density Wave State of $La_3Ni_2O_7$

Ge He[1,10]✉, Jun Shen[1]✉, Shiyu Xie[2,10], Haotian Zhang[1], Mengwu Huo[3], Jun Shu[4], Deyuan Hu[3], Xiaoxiang Zhou[5], Yanmin Zhang[6], Lei Qin[6], Liangxin Qiao[2], Hengjie Liu[2], Chuansheng Hu[2], Xijie Dong[4], Dengjing Wang[4], Jun Liu[1], Wei Hu[7], Jie Yuan[7,8], Yajun Yan[5], Zeming Qi[2], Kui Jin[7,8,9], Zengyi Du[5]✉, Meng Wang[3], Donglai Feng[5]✉

[1] *School of Mechanical Engineering, Beijing Institute of Technology, Beijing 100081, China*

[2] *National Synchrotron Radiation Laboratory, University of Science and Technology of China, Hefei, Anhui 230029, China*

[3] *Center for Neutron Science and Technology, Guangdong Provincial Key Laboratory of Magnetoelectric Physics and Devices, School of Physics, Sun Yat-Sen University, Guangzhou 510275, China*

[4] *Department of Applied Physics, Wuhan University of Science and Technology, Wuhan 430081, China*

[5] *Hefei National Laboratory, and New Cornerstone Science Laboratory, Hefei, Anhui 230088, China*

[6] *Beijing Key Laboratory for Sensor, Beijing Information Science and Technology University, Beijing 100192, China*

[7] *Beijing National Laboratory for Condensed Matter Physics, Institute of Physics, Chinese Academy of Sciences, Beijing 100190, China*

[8] *School of Physical Sciences, University of Chinese Academy of Sciences, Beijing 100049, China*

[9] *Songshan Lake Materials Laboratory, Dongguan, Guangdong 523808, China*

[10] *These authors contributed equally: Ge He and Shiyu Xie*

✉ *e-mail: ge.he@bit.edu.cn; jshen@bit.edu.cn; duzengyi@hfnl.cn; dlfeng@hfnl.cn*

A. Raman selection rules and Raman-active phonons

$La_3Ni_2O_7$ at ambient pressure belongs to space group *Amam* with D_{2h} point group [1]. The factor group symmetry analysis indicates that the Raman phonon modes at Brillouin zone (BZ) center Γ should be decomposed into 36 irreducible representations, $\Gamma_{Raman} = 10A_g + 12B_{1g} + 7B_{2g} + 7B_{3g}$. We adopted the lattice parameters a = 5.450 Å, b = 5.398 Å, c = 20.561 Å, and the Wyckoff positions (La1 4c, La2 8g, Ni 8g, O1 8e, O2 8e, O3 8g and O4 4c) [2]. The Raman tensors R_μ (μ =$A_{\rm g}$, $B_{1\rm g}$, $B_{2\rm g}$, $B_{3\rm g}$) corresponding to the symmetry group are expressed in the xyz coordinates as:

$$A_{\rm g} = \begin{pmatrix} a & 0 & 0 \\ 0 & b & 0 \\ 0 & 0 & c \end{pmatrix}, B_{1\rm g} = \begin{pmatrix} 0 & d & 0 \\ d & 0 & 0 \\ 0 & 0 & 0 \end{pmatrix},$$
$$B_{2\rm g} = \begin{pmatrix} 0 & 0 & e \\ 0 & 0 & 0 \\ e & 0 & 0 \end{pmatrix}, B_{3\rm g} = \begin{pmatrix} 0 & 0 & 0 \\ 0 & 0 & f \\ 0 & f & 0 \end{pmatrix}. \tag{1}$$

The Raman scattering intensity can be deduced as:

$$\boldsymbol{I} \propto |e_{\rm i} \cdot \boldsymbol{R_\mu} \cdot \boldsymbol{e_{\rm s}}|^2. \tag{2}$$

where $\boldsymbol{e_{\rm i}}$ and $\boldsymbol{e_{\rm s}}$ are the unit polarization vectors of the incident and scattered light, respectively. According to the polarization selection rules, the peaks appearing under (xx and $x'x'$) configurations are $A_{\rm g}$ modes, while the peaks appearing under (xy) polarization configuration should be $B_{1\rm g}$ modes. The electronic Raman response is analyzed within the D_{4h} point group, under which the B_{1g} phonon modes of the D_{2h} crystal symmetry appear in the B_{2g} channel. This convention is adopted for consistency with the pseudo-tetragonal symmetry of the electronic structure.

To perform a quantitative analysis of the phonons, we utilize Voigt functions to fit these peaks, which is a convolution of a Guassian and a Lorenz function. The temperature dependent phonon linewidth is simulated with an anharmonic symmetric decay model [3],

$$\Gamma_i(T) = \Gamma_{i,0}\left[1 + \frac{2\lambda_{i,\rm ph-ph}}{\exp\left(\frac{\hbar\omega_0}{2k_BT}\right) - 1}\right] \tag{3}$$

where $\lambda_{i,\rm ph-ph}$ is the phonon-phonon coupling constant, and ω_0 is the corresponding phonon frequency at zero temperature.

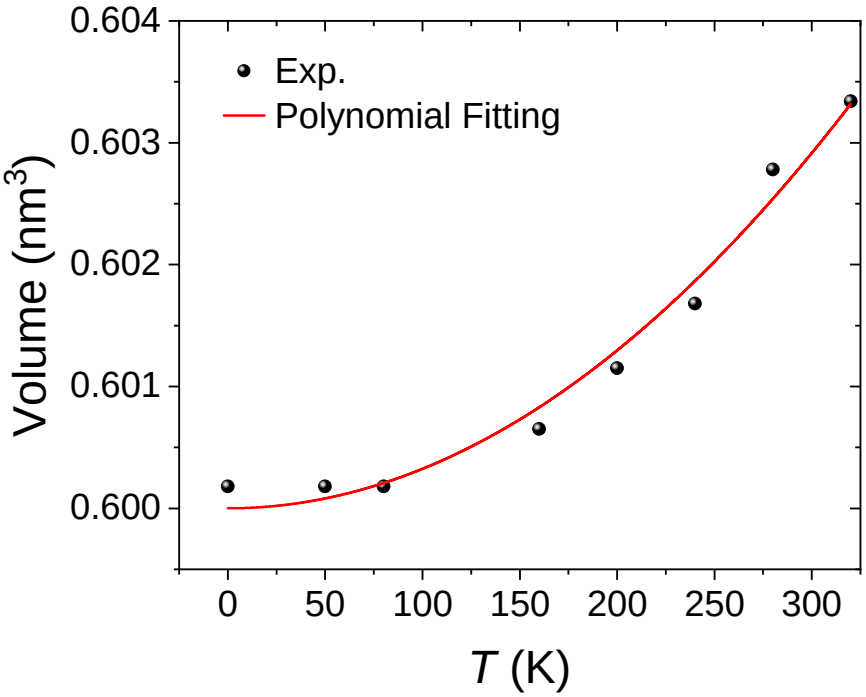

Figure S1. **Temperature dependent volume of $La_3Ni_2O_7$.** The data are adapted from Ref. [5].

The phonon energy shift depends on both the anharmonic decay and the thermal expansion. With taking both into account, the temperature dependence of the phonon energy $\omega_i(T)$ can be given by [4]:

$$\omega_i(T) = \omega_{i,0} + \omega_{i,0}\left\{\exp\left[-3\gamma_i\int_0^T \alpha_V(T')dT'\right] - 1 - \left(\frac{\Gamma_{i,0}}{\sqrt{2}\omega_{i,0}}\right)^2\left[1 + \frac{4\lambda_{i,\mathrm{ph-ph}}}{\exp\left(\frac{\hbar\omega_{i,0}}{2k_BT}\right) - 1}\right]\right\} \quad (4)$$

where γ_i is the Grüneisen parameter of the mode i, and $\alpha_V(T')$ is the coefficient of volume thermal expansion at temperature T'. The volume thermal expansion of $La_3Ni_2O_7$ are plotted in Fig. S1, which adopt from Supplementary Materials of Ref. [5].

Figure S2 presents the Raman spectra and the corresponding fitting parameters for the A_g and B_{1g} phonons as a function of temperature. Our analysis focuses on the prominent Raman-active phonons, namely, the $A_g^{(1)}$, $A_g^{(2)}$, and $B_{1g}^{(3)}$ modes. As shown in Fig. S2 **a** and **b**, these phonon modes are well described by the Voigt function. The extracted phonon frequencies and linewidths as a function of temperature are plotted in Fig. S2 **c** and **d**. The observed temperature dependence can be explained well by thermal expansion within the framework of Grüneisen theory and by anharmonic decay, respectively (see green and red lines in Fig. S2 **c** and **d**).

The absence of any observable phonon anomalies argues against the CDW order as the leading instability in $La_3Ni_2O_7$. Usually, a CDW transition is typically accompanied by periodic lattice

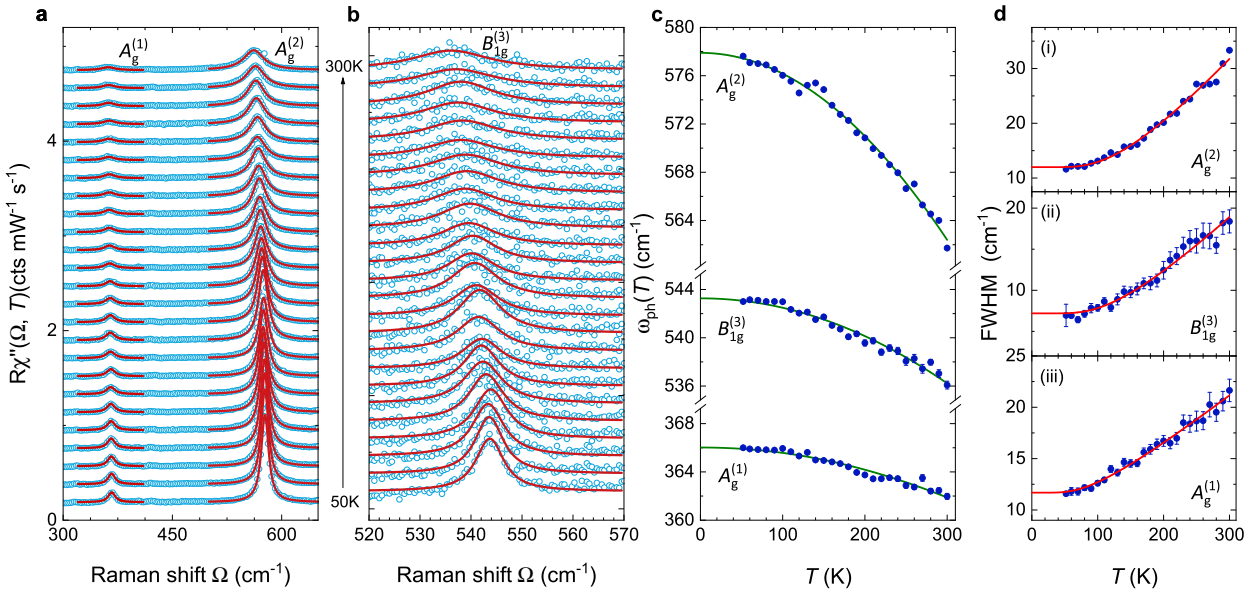

Figure S2. **Raman-active phonons in both the A_g and B_{1g} symmetries.** **a** and **b** Raman response at temperatures ranging from 50 K to 300 K. The spectra other than the one at 50 K are consecutively offset by 0.19 cts s^{-1} mW^{-1} for clarify. The opened blue circles are experimental data. The red curves are Voigt fits. **c** and **d** The plots of phonon energies ω_{ph} and line widths (FWHM) of the three lines as a function of temperature. The green lines in **c** are derived from the volume expansion using Grüneisen theory. The phonon line widths are fitted using an anharmonic model (red lines in **d**). The zero temperature phonon frequency ω_i^0, Grüneisen parameter γ_i, zero-temperature linewidth Γ_i^0, and phonon-phonon coupling constant $\lambda_{i,ph-ph}$ are listed in Tab. I.

Table I. **Phonon parameters of $La_3Ni_2O_7$.** The phonon frequencies ω_i^0, linewidths Γ_i^0, the phonon-phonon coupling parameters $\lambda_{i,\mathrm{ph-ph}}$ and the Grüneisen constants γ_i of the Raman-active $A_g^{(1)}$, $B_{1g}^{(3)}$, and $A_g^{(2)}$ phonons are obtained from the fittings.

Phonons	ω_i^0(cm^{-1})	Γ_i^0 (cm^{-1})	$\lambda_{i,ph-ph}$	γ_i
$A_g^{(1)}$	366.0	11.7	0.57	0.74
$B_{1g}^{(3)}$	543.3	7.2	2.18	0.88
$A_g^{(2)}$	578.0	11.9	2.4	1.84

reconstruction [6, 7], leading to phonon anomalies at the transition temperature and the appearance of multiple zone-folded phonon modes in the Raman spectra below the transition temperature [8–10]. Moreover, the CDW amplitude mode, commonly observed in typical CDW materials such as 2H-$NbSe_2$ [11], $ErTe_3$ [12], and CsV_3Sb_5 [10], is also not detected in $La_3Ni_2O_7$.

B. Extraction of pure A_{1g} Raman response

To isolate the pure A_{1g} Raman response, we performed polarization-resolved measurements in multiple scattering geometries and utilized the symmetry decomposition based on the pseudo-tetragonal D_{4h} point group. Specifically, the A_{1g} component was extracted by combining spectra from parallel polarizations [$xx(A_{1g} + B_{1g})$ and $x'x'(A_{1g} + B_{2g})$] and subtracting contributions from cross polarizations [$xy(B_{2g})$ and $x'y'(B_{1g})$], assuming negligible mixing due to sample misalignment or optical leakage.

The extraction procedure follows:

$$\chi''_{A_{1g}}(\Omega) = \chi''_{xx}(\Omega) + \chi''_{x'x'}(\Omega) - \chi''_{xy}(\Omega) - \chi''_{x'y'}(\Omega), \tag{5}$$

where $\chi''_{ij}(\Omega)$ denotes the Raman response measured in the i-j polarization configuration. This approach effectively removes the B_{1g} and B_{2g} components, isolating the A_{1g} contribution under the assumption of ideal symmetry and linear superposition.

C. The temperature-dependent electronic Raman response in $La_3Ni_2O_7$

To study the evolution of the gap closing with increasing temperature, we present the temperature dependence of Raman spectra and difference spectra [$\Delta\chi''(\Omega, \mathrm{T}) = \chi''(\Omega, \mathrm{T}) - \chi''(\Omega, 160\ \mathrm{K})$] in both the B_{1g} and B_{2g} symmetries, as shown in Fig. S3. The redistribution of the spectral weight gradually decreases and completely disappears at approximately 150 K, indicating that the SDW gap fully closes above this temperature.

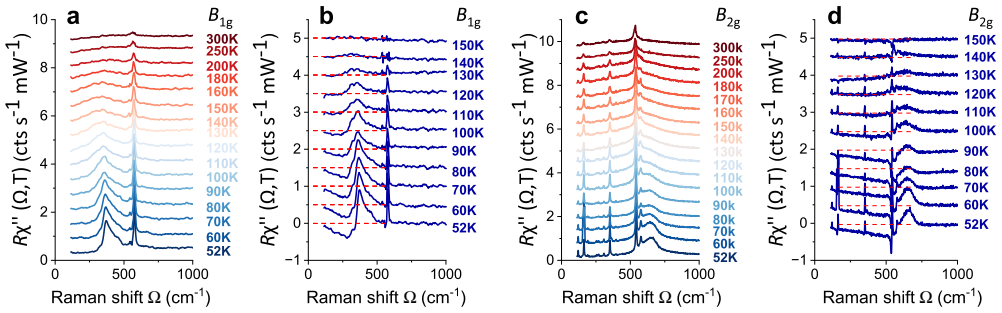

Figure S3. **Electronic Raman spectra in B_{1g} and B_{2g} symmetries.** **a** and **c** Temperature-dependent Raman spectra in the B_{1g} and B_{2g} symmetries at selected temperatures. **b** and **d**, Corresponding difference spectra using the 160 K spectrum as the reference for B_{1g} and B_{2g} symmetries, respectively. Red dashed lines mark the zero-intensity baselines. All spectra are vertically offset for clarity.

D. The fitting results of the electronic Raman response in $La_3Ni_2O_7$

The Raman spectra in B_{1g} and B_{2g} symmetries are fitted using phenomenological models combining Drude and Tsuneto-Maki or Lorentz functions, respectively (see Fig. S4 and Fig. S5). These models successfully capture the redistribution of spectral weight below the SDW transition temperature near 150 K. The B_{1g} channel shows an asymmetric lineshape best described by the Tsuneto-Maki function, indicating a weak-coupling SDW gap at the β' pocket, while the B_{2g} channel exhibits a more symmetric response, fitted with a Lorentz profile consistent with a stronger SDW gap at the β pocket.

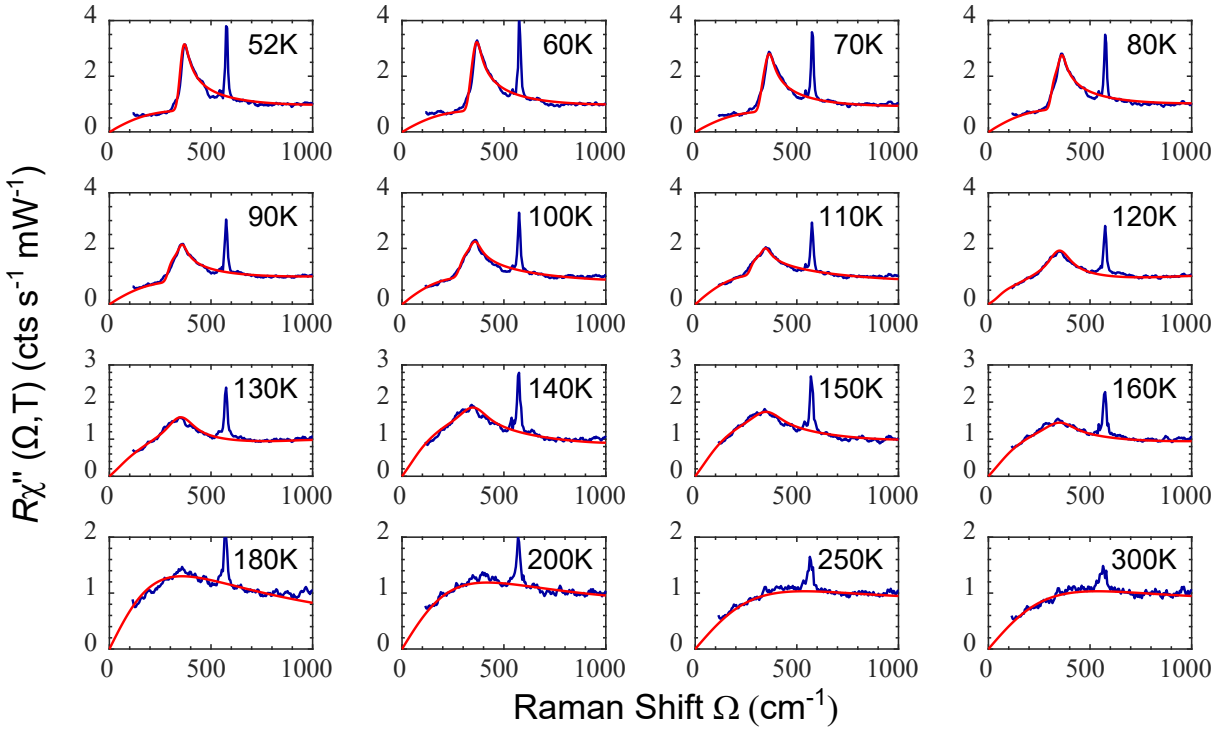

Figure S4. **Fit of the electronic Raman spectra in B_{1g} symmetry.** Raman spectra at various temperatures are fitted using a combined Drude and Tsuneto-Maki model, capturing both the broad background and the asymmetric peak associated with the SDW gap. The experimental data are shown as red lines, while the total fit is overlaid in blue.

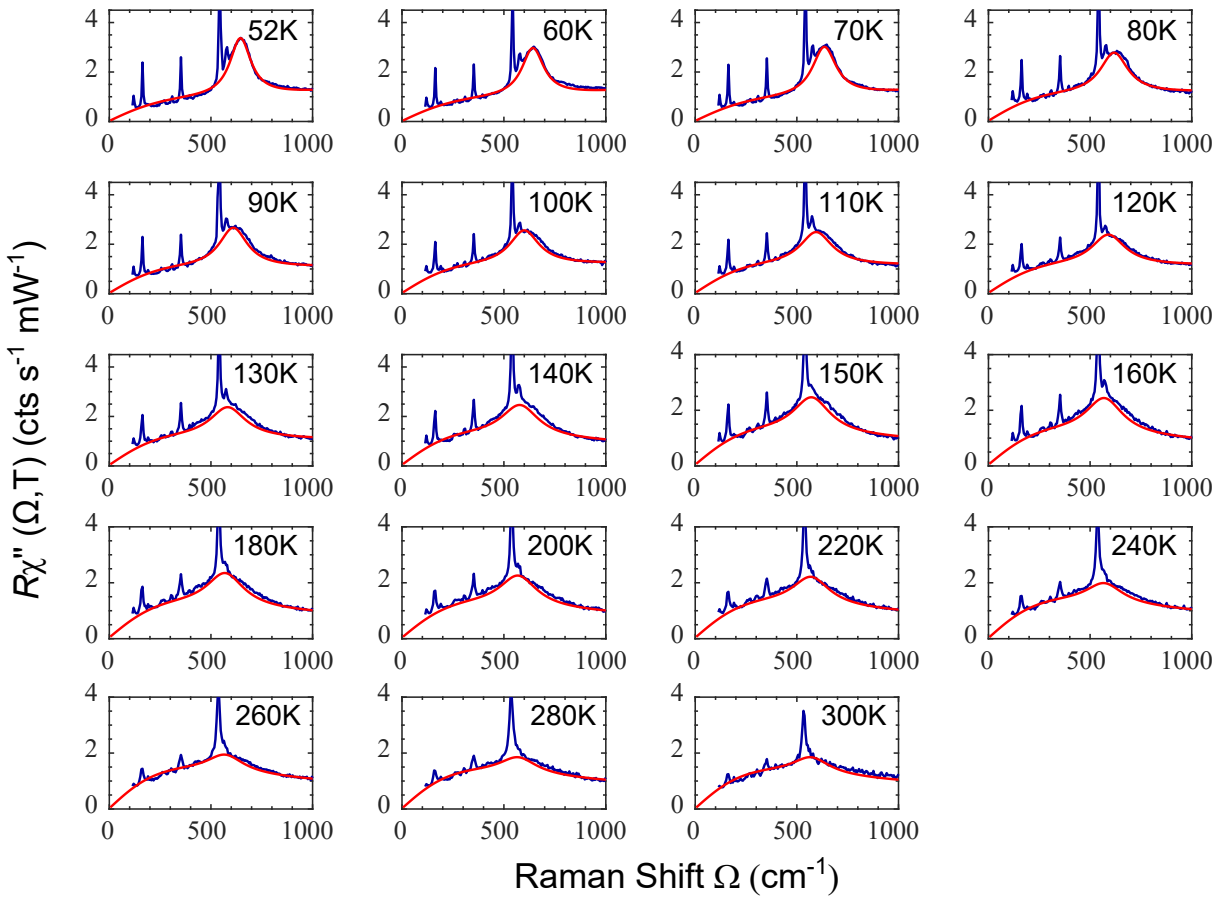

Figure S5. **Fit of the electronic Raman spectra in B_{2g} symmetry.** Raman spectra at various temperatures are fitted using a combined Drude and Lorentz model, capturing both the broad background and the nearly symmetric peak.

E. Tight-binding band structure

The band structure presented in the main text is calculated using an 8-band tight-binding model adopted from Ref. [13]. This model accounts for electron hopping within the two Ni-O layers, where each layer contains two Ni atoms. Each Ni atom contributes two orbitals, namely $d_{x^2-y^2}$ and d_{z^2}.

The Hamitonioun can be described in the basis $(d_x^{At}\ d_z^{At}\ d_x^{Bt}\ d_z^{Bt}\ d_x^{Ab}\ d_z^{Ab}\ d_x^{Bb}\ d_z^{Bb})$ as:

$$\hat{H} = \begin{pmatrix} H_{11}(\mathbf{k}) & 0 & H_{13}(\mathbf{k}) & (H_{14}(\mathbf{k}) & t_\perp^x & 0 & 0 & H_{18}(\mathbf{k}) \\ 0 & H_{22}(\mathbf{k}) & H_{14}(\mathbf{k}) & H_{24}(\mathbf{k}) & 0 & t_\perp^z & H_{18}(\mathbf{k}) & 0 \\ H_{13}^*(\mathbf{k}) & H_{14}^*(\mathbf{k}) & H_{11}(\mathbf{k}) & 0 & 0 & H_{18}^*(\mathbf{k}) & t_\perp^x & 0 \\ H_{14}^*(\mathbf{k}) & H_{24}^*(\mathbf{k}) & 0 & H_{22}(\mathbf{k}) & H_{18}^*(\mathbf{k}) & 0 & 0 & t_\perp^z \\ t_\perp^x & 0 & 0 & H_{18}^*(\mathbf{k}) & H_{11}(\mathbf{k}) & 0 & H_{13}(\mathbf{k}) & H_{14}(\mathbf{k}) \\ 0 & t_\perp^z & H_{18}^*(\mathbf{k}) & 0 & 0 & H_{22}(\mathbf{k}) & H_{14}(\mathbf{k}) & H_{24}(\mathbf{k}) \\ 0 & H_{18}(\mathbf{k}) & t_\perp^x & 0 & H_{13}^*(\mathbf{k}) & H_{14}^*(\mathbf{k}) & H_{11}(\mathbf{k}) & 0 \\ H_{18}(\mathbf{k}) & 0 & 0 & t_\perp^z & H_{14}^*(\mathbf{k}) & H_{24}^*(\mathbf{k}) & 0 & H_{22}(\mathbf{k}) \end{pmatrix} \tag{6}$$

with $H_{11/22}(\mathbf{k}) = \epsilon^{x/z} + 2(t_2'^{x/z}\cos k_X + t_2{}^{x/z}\cos k_Y) + 4t_5{}^{x/z}\cos k_X \cos k_Y$, $H_{13/24}(\mathbf{k}) = 2\cos\frac{1}{2}k_X$ $(t_1{}^{x/z}e^{i\frac{1}{2}k_Y} + t_1'{}^{x/z}e^{-i\frac{1}{2}k_Y})$ and $H_{14/18}(\mathbf{k}) = 2i\sin\frac{1}{2}k_X(t_{3/4}{}^{xz}e^{i\frac{1}{2}k_Y} - t_{3/4}'{}^{xz}e^{-i\frac{1}{2}k_Y})$, where k_X and k_Y are defined as $k_X = k_x + k_y$ and $k_Y = -k_x + k_y$. Here, A and B label the two Ni atoms occupying in the same layer. t and b indicate the top and bottom layer, respectively. x and z stand for the $d_{x^2-y^2}$ and d_{z^2} orbitals. The band dispersion is given by diagonalizing the Hamitonioun as,

$$E_n(\mathbf{k}) = U_n(\mathbf{k})\hat{H}U_n^*(\mathbf{k}) \tag{7}$$

where $U_n(\mathbf{k})$ is the normalized eigen vector.

Figure S6 shows the reproduced band structure as reported in Ref. [13]. Among these, Band 3 and Band 4 cross the Fermi level and form the hole pockets centered at the X_1 points and the electron pockets centered at the Γ, X, Y, and M points, respectively (see Fig. S7).

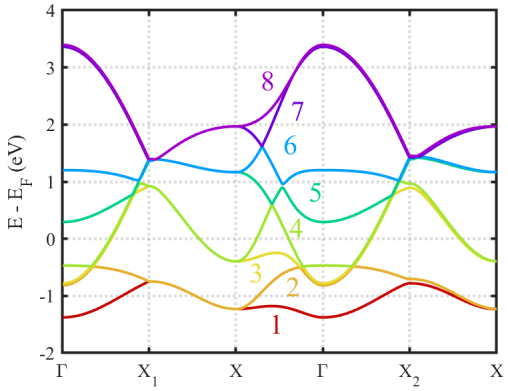

Figure S6. **Band structure along high-symmetric paths calculated using a tight-binding model.** The band indices are labeled in the figure. Band 3 and band 4 cross the Fermi level.

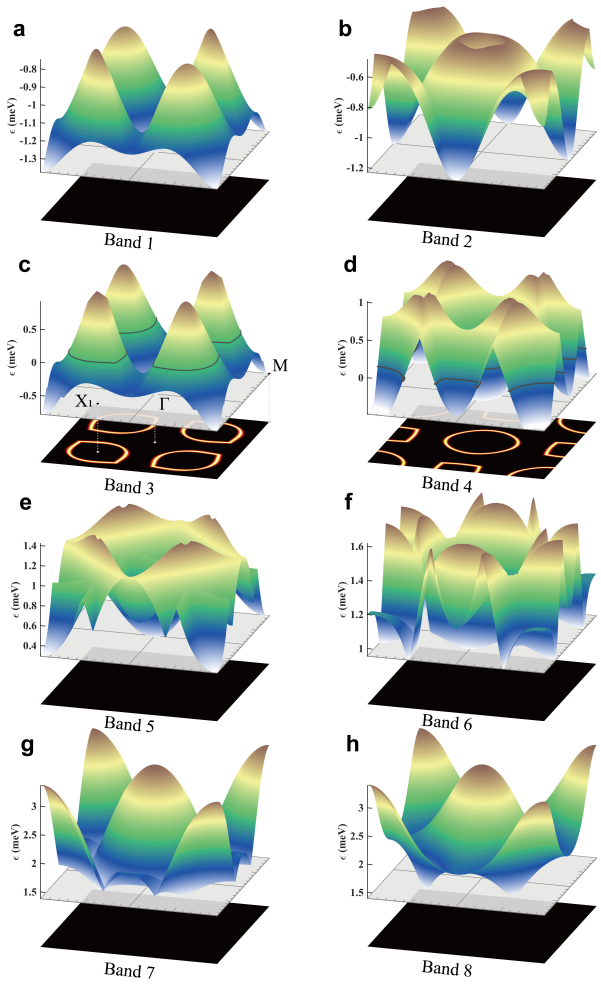

Figure S7. **Band dispersion in 3D view.** The bands are projected onto the Fermi-energy plane. The resulting Fermi pockets are highlighted in panels **c** and **d**.

[1] H. Sun, M. Huo, X. Hu, J. Li, Z. Liu, Y. Han, L. Tang, Z. Mao, P. Yang, B. Wang, J. Cheng, D.-X. Yao, G.-M. Zhang, and M. Wang, Signatures of superconductivity near 80 K in a nickelate under high pressure, Nature **621**, 493 (2023).

[2] Y. Meng, Y. Yang, H. Sun, S. Zhang, J. Luo, L. Chen, X. Ma, M. Wang, F. Hong, X. Wang, and X. Yu, Density-wave-like gap evolution in $La_3Ni_2O_7$ under high pressure revealed by ultrafast optical spectroscopy, Nat. Commun. **15**, 10408 (2024).

[3] P. G. Klemens, Anharmonic decay of optical phonons, Phys. Rev. **148**, 845 (1966).

[4] H. Eiter, P. Jaschke, R. Hackl, A. Bauer, M. Gangl, and C. Pfleiderer, Raman study of the temperature and magnetic-field dependence of the electronic and lattice properties of mnsi, Phys. Rev. B **90**, 024411 (2014).

[5] H. Wang, H. Zhou, and W. Xie, Temperature-dependent structural evolution of ruddlesden–popper bilayer nickelate $La_3Ni_2O_7$, Inorg. Chem. **64**, 828 (2025).

[6] K. Rossnagel, On the origin of charge-density waves in select layered transition-metal dichalcogenides, J. Phys.: Condens. Matter **23**, 213001 (2011).

[7] G. Grüner, *Density Waves in Solids* (Perseus, Cambridge, MA, 1994).

[8] R. Samnakay, D. Wickramaratne, T. R. Pope, R. K. Lake, T. T. Salguero, and A. A. Balandin, Zone-folded phonons and the commensurate–incommensurate charge-density-wave transition in $1\,T - TaSe_2$ thin films, Nano Lett. **15**, 2965 (2015).

[9] O. R. Albertini, R. Zhao, R. L. McCann, S. Feng, M. Terrones, J. K. Freericks, J. A. Robinson, and A. Y. Liu, Zone-center phonons of bulk, few-layer, and monolayer $1\,T - TaS_2$: Detection of commensurate charge density wave phase through Raman scattering, Phys. Rev. B **93**, 214109 (2016).

[10] G. He, L. Peis, E. F. Cuddy, Z. Zhao, D. Li, Y. Zhang, R. Stumberger, B. Moritz, H. Yang, H. Gao, T. P. Devereaux, and R. Hackl, Anharmonic strong-coupling effects at the origin of the charge density wave in CsV_3Sb_5, Nat. Commun. **15**, 1895 (2024).

[11] M.-A. Méasson, Y. Gallais, M. Cazayous, B. Clair, P. Rodière, L. Cario, and A. Sacuto, Amplitude higgs mode in the $2H - NbSe_2$ superconductor, Phys. Rev. B **89**, 060503 (2014).

[12] H.-M. Eiter, M. Lavagnini, R. Hackl, E. A. Nowadnick, A. F. Kemper, T. P. Devereaux, J.-H. Chu, J. G. Analytis, I. R. Fisher, and L. Degiorgi, Alternative route to charge density wave formation in multiband systems, Proc. Natl. Acad. Sci. **110**, 64 (2013).

[13] Y. Wang, K. Jiang, Z. Wang, F.-C. Zhang, and J. Hu, Electronic and magnetic structures of bilayer $La_3Ni_2O_7$ at ambient pressure, Phys. Rev. B **110**, 205122 (2024).